Improving Annual Energy Production of Doubly-Fed Induction Generators

Wang, Xuezhou; Liu, Dong; Polinder, Henk

DOI
10.1109/TEC.2021.3063478

Publication date
2021

Document Version
Accepted author manuscript

Published in
IEEE Transactions on Energy Conversion

This article has been accepted for publication in a future issue of this journal, but has not been fully edited. Content may change prior to final publication. Citation information: DOI 10.1109/TEC.2021.3063478, IEEE Transactions on Energy Conversion

Improving Annual Energy Production of Doubly-Fed Induction Generators

Xuezhou Wang, *Member, IEEE,* Dong Liu, *Member, IEEE,* and Henk Polinder, *Senior Member, IEEE*

***Abstract*—Doubly fed induction generator (DFIG) based wind turbines are most employed for onshore applications because of their cost-effectiveness. The drivetrain improvement is barely studied due to the maturity of the DFIG based systems. This paper investigates two methods for improving the annual energy production (AEP) of the DFIG based wind turbines. They are referred to as short-circuited and △-Y-connected DFIGs. The origins of the AEP improvement are elaborated from the drivetrain perspective. The improvement is quantified by the aerodynamic model of the turbine and the steady-state model of the DFIG. The two methods are then compared when applied to six regions with different wind speed distributions. The AEP improvements at six regions are evaluated and compared to derive the feasibility of the methods for different locations.**

***Index Terms*—Doubly-fed induction generator (DFIG), annual energy production (AEP), aerodynamic model, Delta-Y connection, short-circuited connection.**

I. Introduction

WIND energy capacity installed worldwide has been growing significantly over the last couple of decades. Meanwhile, wind turbine technology is continuously developing. New technologies are emerging, such as superconducting wind generators [1] and brushless doubly-fed induction generators (DFIGs) [2]. In the commercial market, permanent magnet (PM) direct drive generators or PM generators with one or two-stage gearboxes are very attractive for large-scale offshore applications. This is mainly due to the simplified drivetrain system and the increased annual energy production (AEP) [3]. However, for onshore applications, the DFIG drivetrain with a three-stage gearbox and a partially rated power converter (shown in Fig. 1) is still the most employed because it is cost-effective [4].

On the other hand, this fractionally rated power converter leads to some special technical issues for the DFIG drivetrain. For instance, compared to the drivetrain with a full-scale power converter, the low voltage ride through (LVRT) capability is more complicated to analyze [5] and control [6]. Another important issue that comes up with the partially rated converters is power quality. This is because the stator of DFIGs is connected to the grid directly, and the distorted grid voltage may introduce harmonics in the stator currents. This issue is normally solved by using passive LCL filters on the grid-side converters [7] or by some control strategies for harmonic currents suppression [8], [9]. Most literature works on the control aspects related to the grid code requirements.

X. Wang and H. Polinder are with the Department of Maritime and Transport Technology, Delft University of Technology, Delft, The Netherlands, (email: x.wang-3@tudelft.nl, h.polinder@tudelft.nl).

D. Liu is with the College of Energy and Electrical Engineering, Hohai University, Nanjing, China, (email: dongliu@hhu.edu.cn).

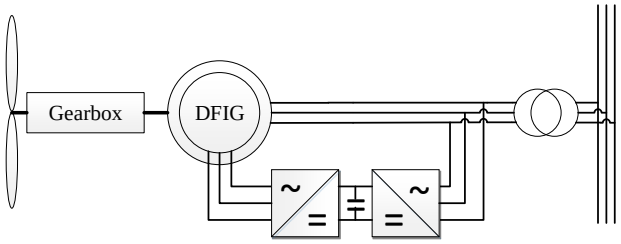

Fig. 1. Scheme of a DFIG drivetrain concept

However, there are not many papers working on how to improve the AEP of DFIGs. Most of them focus on the well-known maximum power point tracking (MPPT) algorithm [10]. Moreover, the control strategy for minimizing losses is studied in [11]. A control scheme combining the loss minimization strategy and MPPT is proposed for higher energy production [12]. From the generator's perspective, it is difficult to increase its efficiency by means of magnetic-flux weakening control methods because the stator is directly connected to the grid [13]. Two methods are proposed to lower the magnetizing losses of the DFIGs [14]. The first one is to short-circuit the stator at low loads, and all electrical power transfers through the rotor to the grid. The improvement of the generator efficiency and the generator control strategy are addressed in [15]. The possibility of extending the operating speed range is mentioned, but not evaluated in detail. The second one is to keep the stator △-connected at high loads, but Y-connected at low loads. There is even less literature studying the second method, although the reference [15] claims that some commercial generator systems have applied the △-Y connection. Although the first operational mode attracts some research interest on its control strategy [16] and even proves to have a better LVRT capability [17], no further literature looks into the influence of either method on the AEP in detail.

The contribution of this paper is to elaborate the above two methods for increasing the AEP and quantify this improvement with the help of the aerodynamic model, the gearbox model, and the steady-state model of DFIGs. Rather than only regarding the generator efficiency in the literature, the origin of how the short-circuited and △-Y-connected DFIGs increase the AEP is explained in detail from the drivetrain system point of view. A comparison is made between these two methods. Moreover, an evaluation is applied to a case

This article has been accepted for publication in a future issue of this journal, but has not been fully edited. Content may change prior to final publication. Citation information: DOI 10.1109/TEC.2021.3063478, IEEE Transactions on Energy Conversion

study DFIG in different areas with different wind resource distributions. The AEP benefits are quantified for helping the manufacturers decide whether it is worth implementing the additional operation modes at the expense of the additional equipment.

This paper starts with an introduction to the original DFIG based drivetrain system. The models of the aerodynamic conversion, the gearbox, and the generator are given and the DFIG steady-state performance is validated by experimental measurements. Next, the ideas and the principles of the △-Y-connected and short-circuited DFIGs, as well as the operating mode switching, are explained. The mechanism of the AEP improvement is then illustrated by using the presented models. Subsequently, an evaluation procedure is applied to several areas with different wind speed distributions. Finally, conclusions are drawn.

II. Original DFIG Based Wind Turbine System

A. Aerodynamic Conversion

Table I gives the parameters of the wind turbine studied. The available shaft power harvested from the wind can be calculated as:

$$P_t = \frac{1}{2}\rho A_r v^3 C_p(\lambda, \theta), \tag{1}$$

where ρ is the mass density of air, v is the wind speed, A_r is the area swept by the turbine rotor, and C_p is the power coefficient or the aerodynamic efficiency. C_p is a function of the tip speed ratio λ given by (2) and the blade pitch angle θ. The theoretical maximum value of C_p is limited by the Betz limit as 0.593.

$$\lambda = \frac{r\Omega_t}{v}, \tag{2}$$

where Ω_t is the angular speed of the turbine rotor. The aerodynamic behavior of the turbine rotor is complicated. It is normally calculated numerically by the manufacturers. Fig. 2 gives the optimal power coefficient with respect to the tip speed ratio for the turbine studied. The pitch angle varies to achieve the optimal power coefficient at each tip speed ratio.

Ideally, the turbine rotor rotates always at the speed with the optimum tip speed ratio (TSR) within the whole wind speed range indicated by the dotted line in Fig. 3. Meanwhile, it always transfers the wind power with the maximum aerodynamic efficiency as shown in Fig. 4. However, there are always lower and upper limits for the turbine rotor speeds

TABLE I
Wind Turbine Parameters

Description	Machine parameter	Value
Nominal turbine power [MW]	P_{nom}	2.5
Turbine rotor radius [m]	r	70
Cut-in wind speed [m/s]		3.5
Nominal rotor speed [rpm]	$\Omega_{t,nom}$	11
Minimal rotor speed [rpm]	$\Omega_{t,min}$	7.3
Optimum tip speed ratio	λ_{opt}	10.2
Maximum aerodynamic rotor efficiency	$C_{p,max}$	0.47
Mass density of air [kg/m^3]	ρ	1.225

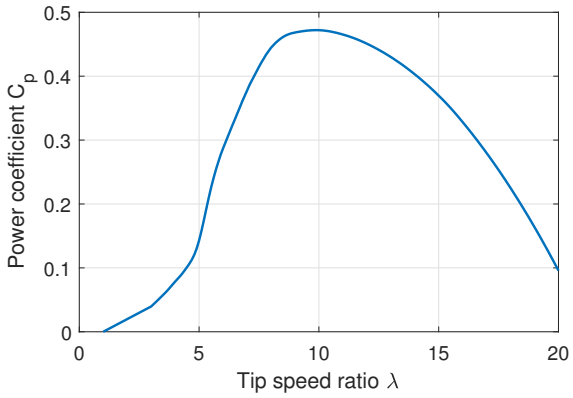

Fig. 2. Power coefficient C_p with respect to tip speed ratio

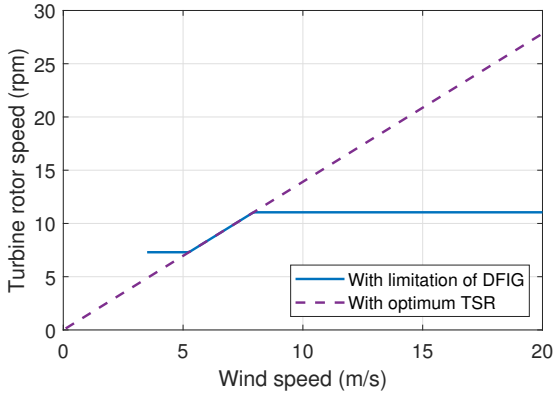

Fig. 3. Turbine rotor speed as a function of wind speed

based on the size of the power converter. In this study, the rating of the converter is 600 kVA resulting in the speed limitations indicated by the solid line in Fig. 3. It shows that the highest turbine rotor speed above the rated wind speed is limited. The blades are pitched to reduce the aerodynamic efficiency as shown in Fig. 4. Therefore, the harvested power is also limited. One thing that might be good to mention here is that the minimum operating speed is about 30% below the synchronous speed while the nominal speed is only about 9% above the synchronous speed. One reason is the limitation of the tip speed of the blade due to the acoustic emission level of the turbine. However, this does not affect the analysis and the conclusion in the following sections.

The stator voltage of the DFIG is always the same as the grid voltage. The rotor voltage increases if the rotating speed of the DFIG moves away from synchronous speed when the slip increases. This rotor voltage is limited by the voltage stress on the power converter. Therefore, the turbine rotor cannot follow its optimal curve but keeps a minimal rotating speed as shown in Fig. 3. Therefore, Fig. 4 indicates that it cannot follow the optimal power coefficient at low wind speeds.

This article has been accepted for publication in a future issue of this journal, but has not been fully edited. Content may change prior to final publication. Citation information: DOI 10.1109/TEC.2021.3063478, IEEE Transactions on Energy Conversion

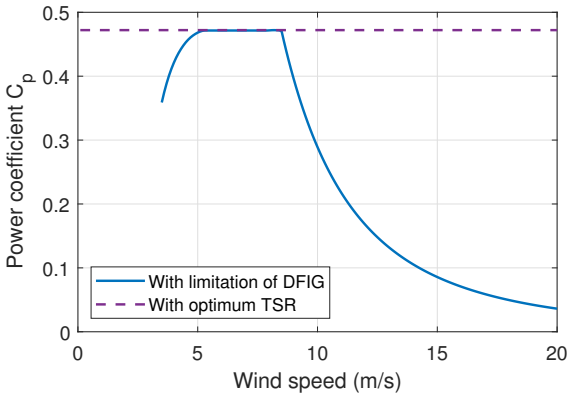

Fig. 4. Power coefficient as a function of wind speed

TABLE II
DFIG PARAMETERS

Description	Machine parameter	Value
Rated power [MW]	$P_{Gen,rate}$	2.6
Rated speed [rpm]	n_{rate}	1635
Number of pole pairs		2
Stator/Rotor winding connection		△/Y
Stator line voltage [V]	U_s	690
Stator outer diameter [mm]	D_{so}	980
Stator inner diameter [mm]	D_{si}	660
Air-gap length [mm]	l_g	3
Rotor inner diameter [mm]	D_{ri}	360
Axial length [mm]	L_{stk}	760

B. Gearbox Modeling

It is necessary to estimate the gearbox losses for predicting its efficiency. [14] presents a way as follows:

$$P_{GB,loss} = \alpha P_t + \beta P_{nom} \frac{\Omega_t}{\Omega_{t,nom}}, \tag{3}$$

where α is the gearbox mesh losses constant and β is the friction constant. For a 2 MW level gearbox, the constants α = 0.02 and β = 0.005 are reasonable according to [18]. The output power of the gearbox or the input power of the generator can be formulated as:

$$P_{GB,out} = P_{Gen,in} = P_t - P_{GB,loss}. \tag{4}$$

C. Generator Modeling

Table II gives the specifications of the studied DFIG. Fig. 5 depicts the electrical equivalent circuit (EEC) model, which is applied to estimate the steady-state performance of the DFIG. Table III summarizes the parameters of the EEC model. The rotor side parameters are referred to the stator side.

The output power of the DFIG is calculated by:

$$\begin{aligned} P_{Gen,out} &= P_s + P_r \\ &= P_{Gen,in} - P_a - P_m - P_{Fes} - P_{Fer} - P_{Cus} - P_{Cur}, \end{aligned} \tag{5}$$

where P_s and P_r are the output power of the stator and rotor, P_a is the stray loss, P_m is the mechanical friction and windage losses, P_{Fes} and P_{Fer} are the stator and rotor iron core losses, P_{Cus} and P_{Cur} are the stator and rotor copper losses. Furthermore, the stator and the rotor active power hold the following relationship:

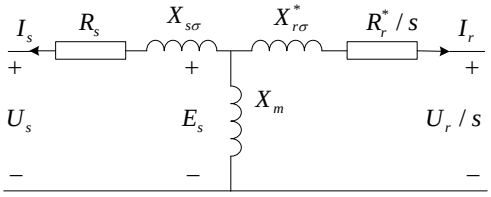

Fig. 5. Steady-state electrical equivalent circuit of the DFIG

TABLE III
ELECTRICAL EQUIVALENT CIRCUIT MODEL PARAMETERS

Description	Machine parameter	Value
Stator resistance [Ω]	R_s	0.0055
Stator leakage reactance [Ω]	$X_{s\sigma}$	0.0470
Rotor resistance [Ω]	R^*_r	0.0061
Rotor leakage reactance [Ω]	$X^*_{r\sigma}$	0.0580
Magnetizing reactance [Ω]	X_m	2.48

TABLE IV
CORE LOSSES COEFFICIENTS

Description	Parameter	Value
Hysteresis loss coefficient [W/kg]	k_h	0.02145
Eddy-current loss coefficient [W/kg]	k_c	0.00014
Excess loss coefficient [W/kg]	k_e	0.00099

$$P_r + P_{Cur} = -s(P_s + P_{Cus}), \tag{6}$$

$$s = \frac{n_s - n_m}{n_s}, \tag{7}$$

where s is the slip, n_s is the synchronous speed and n_m is the mechanical rotating speed of the DFIG.

The stray loss is estimated using the method given in IEC-60034 standard which is also normally adopted in the tests.

$$P_a = (0.025 - 0.005 \cdot \lg P_{Gen,rate}) \times P_{Gen,in}. \tag{8}$$

The sum of the windage and friction losses is calculated by the way given in [19].

$$P_m = k_\rho D_r (l_r + 0.6\tau_p)\nu_r^2, \tag{9}$$

where k_ρ is an experimental factor, D_r is the rotor diameter, l_r is the rotor length, τ_p is the pole pitch and ν_r is the surface speed of the rotor. k_ρ is selected as 6.5 in this study. The iron core losses are predicted by the Bertotti model [20]:

$$\begin{aligned} P_{Fe} &= P_h + P_c + P_e \\ &= k_h f B^2 m + k_c (fB)^2 m + k_e (fB)^{1.5} m, \end{aligned} \tag{10}$$

where m is the weight of the corresponding core part, k_h, k_c, and k_e are the coefficients of the hysteresis, the eddy-current, and the excess losses. The coefficients used in this paper are given in Table IV. The detailed identification of these coefficients using core losses curves provided by the

This article has been accepted for publication in a future issue of this journal, but has not been fully edited. Content may change prior to final publication. Citation information: DOI 10.1109/TEC.2021.3063478, IEEE Transactions on Energy Conversion

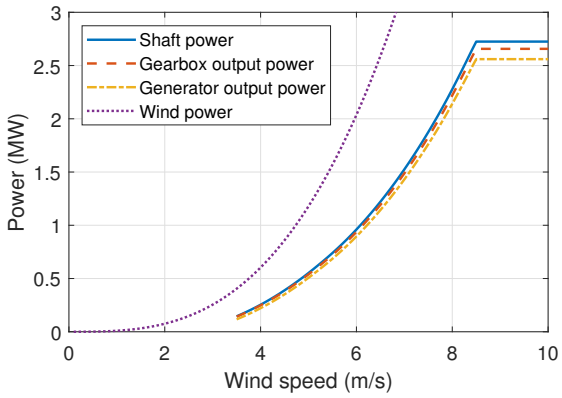

Fig. 6. Power delivered by the DFIG based turbine studied

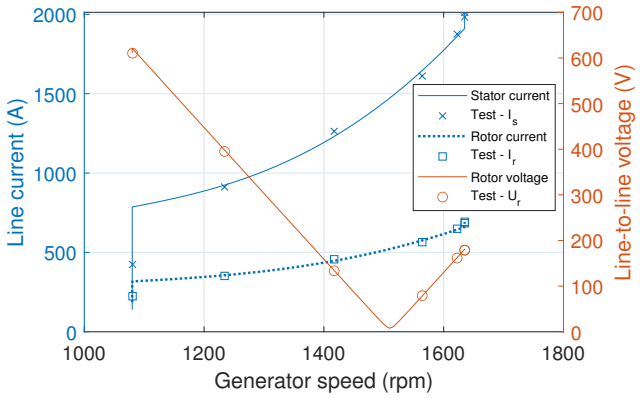

Fig. 8. Measurements of voltage and current

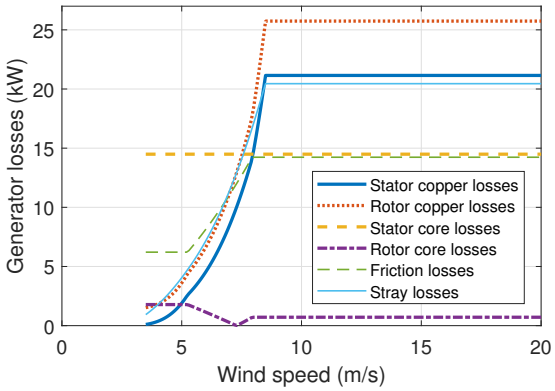

Fig. 7. Losses of the DFIG

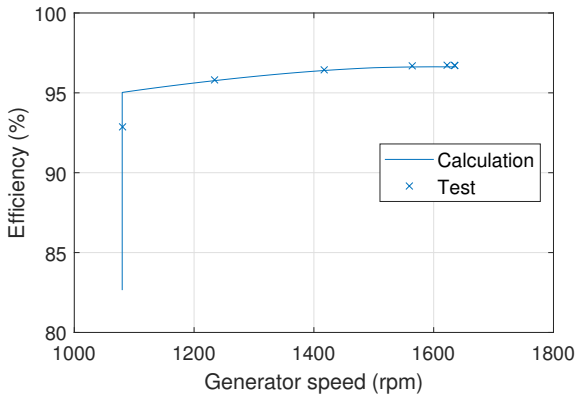

Fig. 9. Measurements of generator efficiency

lamination manufacturer can be found in [20]. The magnetic flux level is closely linked to the stator terminal voltage which is fixed by the grid. The stator frequency is also fixed at 50 Hz. Therefore, it is reasonable to assume that the stator core losses are approximately constant within the whole operating range. However, the rotor frequency varies with speed. The rotor core losses can then be calculated as:

$$P_{Fer} = \left|\frac{s}{s_0}\right| P_{hr}^{rated} + \left|\frac{s}{s_0}\right|^2 P_{cr}^{rated} + \left|\frac{s}{s_0}\right|^{1.5} P_{er}^{rated}, \quad (11)$$

where s_0 is the rated slip (-0.09 in this case), P_{hr}^{rated}, P_{cr}^{rated}, and P_{er}^{rated} are the corresponding losses at the rated operation point. It is straightforward to calculate the copper losses once the stator and rotor currents are solved by the EEC model:

$$P_{Cus} = 3I_s^2 R_s, \quad (12)$$

$$P_{Cur} = 3I_r^2 R_r. \quad (13)$$

Fig. 6 gives a zoomed view of the final output power of the DFIG. Furthermore, Fig. 7 shows the generator losses with respect to the wind speed. The stator and rotor copper losses increase when the output power goes up. The friction losses follow a similar pattern of the rotating speeds as shown in Fig. 3. The rotor frequency is so low that the corresponding rotor core losses can be neglected. As mentioned above, the stator core losses are roughly constant. Fig. 7 also indicates the stator core losses dominate at low wind speeds, which is the concern discussed in [14]. Therefore, at the low wind speed range, lowering the core losses could be more significant and useful for improving the generator efficiency.

D. Generator Steady-State Performance Validation

The traditional on-load tests are carried out to validate the above EEC model in the DFIG operating mode. Fig. 8 shows the voltage and current of the stator and the rotor. Both the stator and the rotor currents increase as the electromagnetic torque goes up. The rotor voltage is minimal at the synchronous speed while it is maximal at the cut-in speed. Originally, this generator cannot rotate slower due to the limitation of the rotor voltage. Fig. 9 gives the comparison between the predicted and measured generator efficiency. The on-load measurements validate that the above EEC model estimates the generator steady-state performance accurately. This EEC model would also be applied to predict the steady-state performance of the △-Y-connected and short-circuited DFIGs in the following section. A minor modification for the the △-Y-connected DFIG is to apply $U_s/\sqrt{3}$ instead of U_s to the stator phase voltage when the stator winding shifts from △ to Y connection. This EEC model is also valid for the short-circuited DFIG, but the stator side parameters should be referred to the rotor side. The generator maximum efficiency

This article has been accepted for publication in a future issue of this journal, but has not been fully edited. Content may change prior to final publication. Citation information: DOI 10.1109/TEC.2021.3063478, IEEE Transactions on Energy Conversion

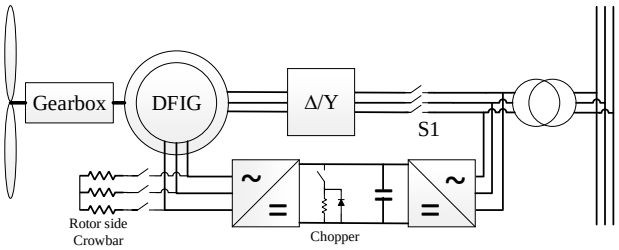

Fig. 10. Scheme of a △-Y-connected DFIG drivetrain

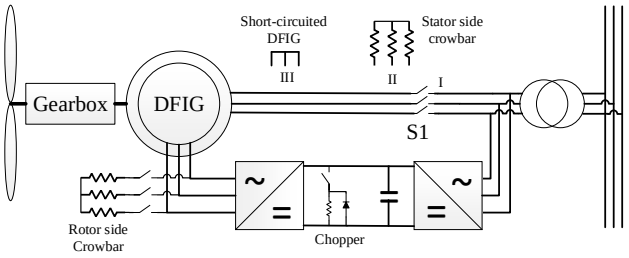

Fig. 11. Scheme of a short-circuited DFIG drivetrain

control strategy is considered for the steady-state calculation in the short-circuited operating mode [21].

III. Improved DFIG Based Systems

This section firstly introduces the principles of two improvement methods. The main changes are on the stator winding side while the original power converter is still there connecting the rotor winding with the grid. The mode switching is then discussed, although it is not the focus of this paper. Finally, the improvement by using the presented methods is compared to the original system from the drivetrain system perspective.

A. △-Y-Connected DFIG

The basic idea of △-Y-connected DFIG is to reduce the stator phase voltage from U_s to $U_s/\sqrt{3}$ by switching the stator winding from △ connection to Y connection. The reduced stator phase voltage leads to lower core losses due to a lower flux level [15]. This helps to achieve a higher generator efficiency at the low wind speed range. The exact value for the low wind speed range will be discussed in section III-D. In addition, the reduced stator phase voltage leads to a lower rotor voltage since the physical turn ratio between stator and rotor windings keeps the same as before. This makes the generator be able to operate at a lower speed. Furthermore, it can also improve the aerodynamic efficiency at the low wind speed range. These three advantages will be explained in detail below. This paper finally finds that extending the operating range and adopting a higher aerodynamic efficiency are much more important than only increasing the generator efficiency.

Fig. 10 gives the scheme of the △-Y-connected DFIG system. The generator operates as a normal DFIG with the △-connected stator winding at the high wind speed range. The stator winding becomes Y-connection at the low-speed range. However, these two modes cannot be switched directly in practice not only due to the voltage amplitude but also the voltage phase angle. The reference [14] simply describes a possible way by reducing the turbine power to zero. The stator winding disconnects and changes the connection. Then the turbine is synchronized to the grid again. This method is crude and the pitch control takes time which may sacrifice some energy production. With the help of the original power converter shown in Fig. 10, it might be not necessary to reduce the turbine power to zero. At the low wind speed (low power), the power converter can quickly control the stator for producing zero active and reactive power. The stator switches the connection after the breaker is open near zero current. Then the converter controls the stator voltage to be synchronized with the grid [22]. For preventing the power converter from being damaged or losing control [5], various switching of internal control and protection circuits in LVRT solutions like the rotor side crowbar and the chopper could be adopted here for the mode switching [23].

B. Short-Circuited DFIG

The basic idea of short-circuited DFIG is to make the generator operate like an ordinary squirrel cage induction generator (SCIG) by short-circuiting the original stator winding. Equivalently, the physical stator acts as the SCIG's 'rotor' and the physical rotor acts as the SCIG's 'stator' connecting to the grid through a power converter. The 'stator' terminal voltage can be controlled for a lower flux level at the low wind speed range resulting in lower core losses. Similar to the previous situation, the exact value for the low wind speed range will be discussed in section III-D. The core losses dominate at the low wind speed range as shown in Fig. 7. This helps to improve the generator efficiency in this operating mode. Moreover, due to the fact that the terminal voltage of the generator side power converter is always under control, this configuration helps the turbine operate at a lower wind speed compared to the △-Y-connected DFIG.

Fig. 11 gives the scheme of the short-circuited DFIG system. Again, it operates as a normal DFIG at the high-speed range. The stator winding is disconnected from the grid and short-connected at low wind speeds The previous method with the help of the original power converter could be still applied here. Ideally, the direct switching is possible in this case since the synchronization between the stator and grid voltages is not a concern anymore. But the direct switching is similar to the stator three-phase full-voltage dip which might lead to unacceptable high rotor voltage and current. Only the rotor side protection as mentioned above may not be enough to prevent this sudden transient process producing a big current and electromagnetic torque. In [24], the dynamic behaviors of the DFIG during three-phase voltage dips have been investigated in detail analytically. If we assume the voltage dip occurs at t_0 moment, the evolution of the stator flux is derived as:

$$\psi_s(t \geqslant t_0) = \frac{U_s}{j\omega_s} e^{j\omega_s t_0} e^{-t/\tau_s}, \tag{14}$$

where $\tau_s = L_s/R_s$ is the time constant. The stator flux decreases exponentially to zero in 3∼5 τ_s. For large generators

This article has been accepted for publication in a future issue of this journal, but has not been fully edited. Content may change prior to final publication. Citation information: DOI 10.1109/TEC.2021.3063478, IEEE Transactions on Energy Conversion

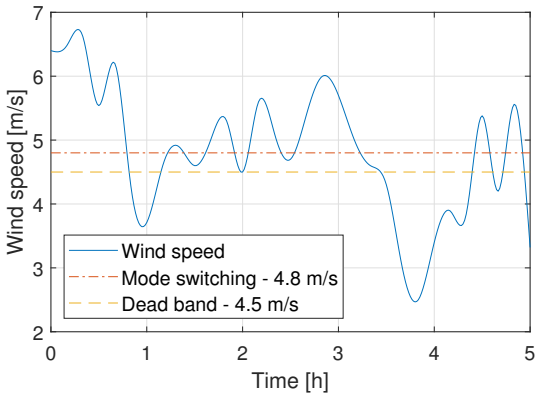

Fig. 12. Dead band of mode switching

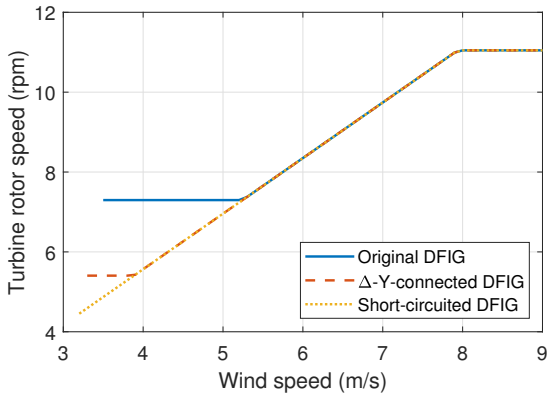

Fig. 13. Improved turbine rotor speed

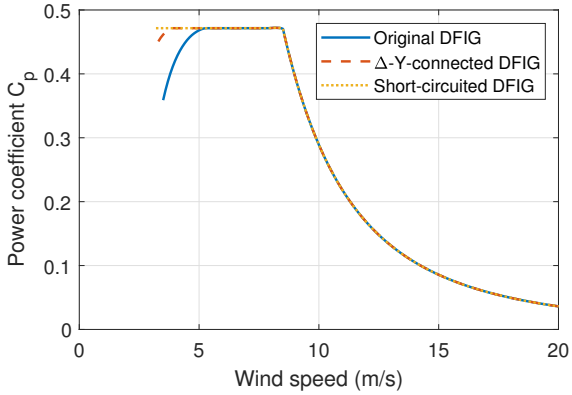

Fig. 14. Improved power coefficient

of 1 MW, this time constant could be up to 1-1.5 s which makes the transient last some seconds [24]. One way of limiting this transient period, as well as the voltage and current, is to connect external impedance like the stator side crowbar shown in Fig. 11 [17], [24]. Therefore, S1 firstly switches from the grid to the stator side crowbar to reduce the transient influence. It then switches to the short-circuited connection when the stator terminal voltage is close to zero.

C. Discussion on Mode Switching

Although two references [17] and [25] have presented the control schemes and indicated that the transient switching process would not exceed the permissible limits, there are few papers that investigate this process in detail. Fortunately, the power converter helps the mode switching at low speed. Moreover, the short-circuited switching has similar characteristics like LVRT to which some LVRT measures could be applied. However, what are the optimized methods and control strategies are open to study. Considering the typical time scale of the power converter control and three-phase voltage dips, it is reasonable to assume that the mode switching could be finished in a couple of seconds. Meanwhile, compared to the operating hours (e.g. >1000 hours annually for the wind between 3.5 m/s and 4.5 m/s in the study below), it is reasonable to estimate the AEP without taking this transient period into account just like neglecting the start-up period.

Another possible concern is the frequent mode switching if the wind speed fluctuates frequently around the switching point. This situation is quite similar to those around the cut-in and cut-out speeds. Fortunately, commercial wind turbines have had available solutions. A small gap around the operating speed, named dead band, is currently widely adopted in practice [26]. In fact, the use of a dead band is quite common in control engineering [27]. The dead band could prevent repeated activation and deactivation cycles and avoid unnecessary control. We take the mode switching of the short-circuited DFIG as an example and explain the basic idea of using the dead band in Fig. 12. This is just a hypothetical wind profile for illustrating the idea. As mentioned before, the short-circuited DFIG mode is switched at the wind speed of 4.8 m/s. Fig. 12 indicates the mode would switch seven times between 1 h and 3 h because the wind speed curve crosses the wind speed curve seven times. If there is a dead band and the operating mode will not switch before the speed decrease below the dead band (e.g. 4.5 m/s), the mode would only switch once when the wind speed increases above 4.8 m/s for the first time at around 1.2 h. The design of the dead band depends on the statistical results of the wind resource measured on-site. Usually, the boundary of the dead band is selected to make its influence on the AEP as small as possible which is almost negligible [26].

D. Comparison with an Original DFIG Drivetrain System

Following the way presented in Section II, the turbine rotor speed, the shaft power, and the generator efficiency are calculated. Fig. 13 gives the turbine rotor speeds with △-Y-connected and short-circuited DFIGs. It indicates that the two improving methods make the turbine not only operate at lower wind speeds, but also follow the curve with the optimal TSR as much as possible. The latter one is even more important, which leads to a higher power coefficient at the low wind speed range as shown in Fig. 14. This can be more clearly observed from the captured shaft power as shown in Fig. 15. The cut-in wind speeds are reduced from 3.5 m/s to 3.3 m/s and 3.2 m/s in this case turbine by using the △-Y-connected and the short-circuited DFIGs, respectively.

This article has been accepted for publication in a future issue of this journal, but has not been fully edited. Content may change prior to final publication. Citation information: DOI 10.1109/TEC.2021.3063478, IEEE Transactions on Energy Conversion

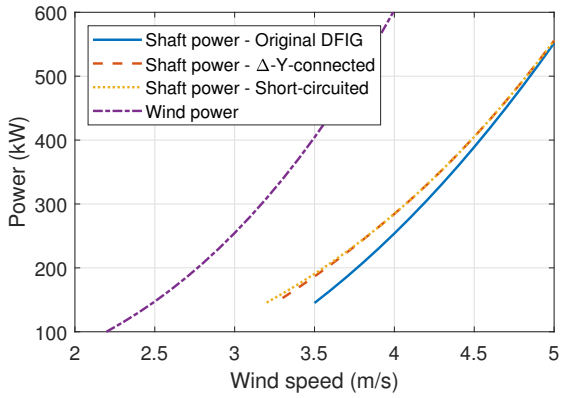

Fig. 15. Improved shaft power captured

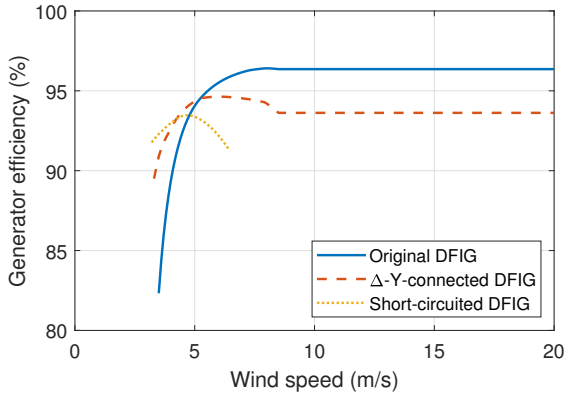

Fig. 16. Comparison of generator efficiency

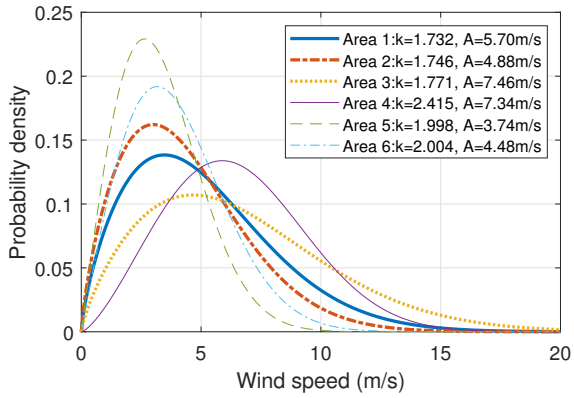

Fig. 17. Annual Weibull distribution of wind speeds

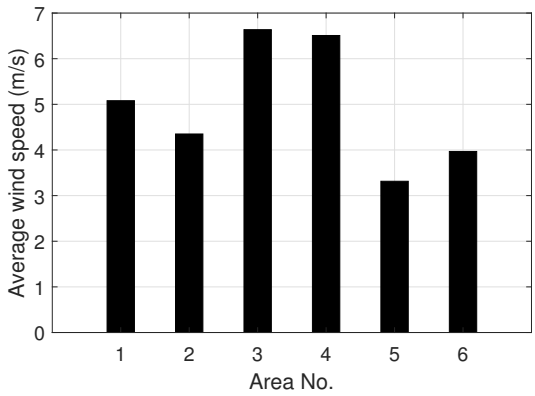

Fig. 18. Annual average wind speeds

Fig. 16 gives the comparison of the generator efficiency using different modes. As expected, the two improving ways both have a higher efficiency at the low wind speed range. The short-circuit mode intersects the original efficiency curve at the wind speed of about 4.8 m/s. It stops at around 6.4 m/s because the generator output power is out of the capacity of the power converter. The △-Y-connection mode intersects the original efficiency curve at around 5.2 m/s and is given for the whole wind speed range. However, showing the efficiency curve in the whole speed range does not make sense for the △-Y-connection mode. That low efficiency at the high wind speed range results in a huge amount of heating which is far beyond the cooling capability of the studied DFIG. In addition, the intersection speeds mentioned are the switching moments between the presented operating modes and the normal DFIG operating mode. Unlike the cut-in speed and the aerodynamic power coefficient, one cannot say whose efficiency is higher between these two modes. It depends on the design of the generator. For the case study DFIG in this paper, the short-circuit mode has a higher efficiency below the wind speed of 4.3 m/s while the △-Y-connection mode is more efficient above 4.3 m/s.

IV. AEP Improvement for Different Areas

As mentioned above, the implementation of the presented operating modes needs additional equipment. Whether it is worth for the wind turbine manufacturers mainly depends on the amount of AEP improvement. An evaluation of AEP for several different areas will be quantified in this section. Some guidelines will then be drawn.

A. Wind Distribution

The frequency distribution of wind speed is given by the Weibull function:

$$f(v) = \frac{k}{A}\left(\frac{v}{A}\right)^{k-1} e^{-(v/A)^k}, \tag{15}$$

where v is the wind speed in m/s, k is the shape parameter (dimensionless), and A is the scale parameter in m/s. The mean wind speed is calculated by:

$$\bar{v} = A \cdot \Gamma\left(1 + \frac{1}{k}\right), \tag{16}$$

where Γ is the Gamma function. The wind speed pattern and energy potential of six different regions in China are studied in [28]. With the given shape and scale parameters, Fig. 17 shows the annual Weibull distribution of the wind speed for these six areas. The annual average wind speed is summarized in Fig. 18. Area 3 and Area 4 have the highest average wind speed of about 6.5 m/s while Area 5 and Area 6 have the lowest wind speed between 3 and 4 m/s.

This article has been accepted for publication in a future issue of this journal, but has not been fully edited. Content may change prior to final publication. Citation information: DOI 10.1109/TEC.2021.3063478, IEEE Transactions on Energy Conversion

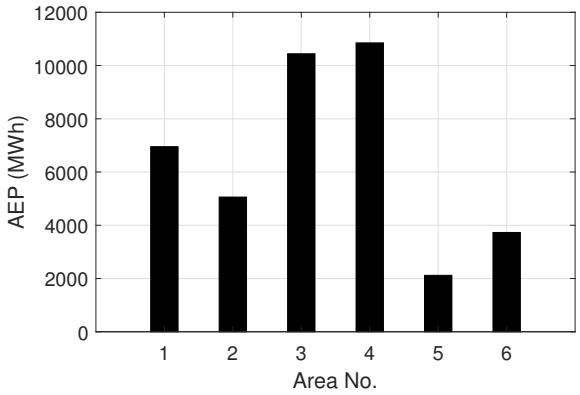

Fig. 19. AEP of original DFIG based drivetrain system

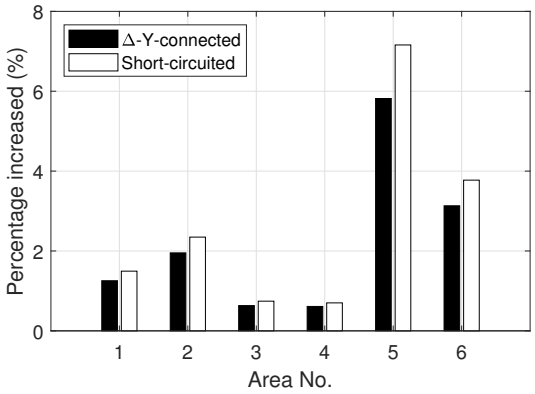

Fig. 20. AEP improvement considering both aerodynamic and generator

B. AEP Evaluation

The AEP of the original DFIG based system is calculated and given in Fig. 19. It agrees with the expectation from the average speeds as shown in Fig. 18. Area 3 and Area 4 have the highest AEP.

Fig. 20 gives the AEP improvement by applying the △-Y-connected and short-circuited DFIGs to these six regions. Firstly, the short-circuited DFIG is always better than the △-Y-connected DFIG. It can be explained by the higher power coefficient and the lower cut-in wind speed as shown in Fig. 14 and 15, respectively. Furthermore, the gap between the improvements using these two methods varies with respect to different areas. The difference between these two methods is not significant in Area 3 and Area 4 with a high average wind speed (6∼7 m/s in this paper). However, the difference is significant for the region with a low average wind speed of about 3.2 m/s as Area 5. On one hand, it means that low wind speed areas would enhance the advantage of the short-circuited DFIG. On the other hand, it essentially indicates that the areas with higher average wind speeds cannot benefit too much by decreasing the cut-in speed or adopting a higher aerodynamic efficiency in the low speed section of the power curve. Compared to the △-Y-connected DFIG, even though the generator efficiency of the short-circuited DFIG is not always higher, it completely makes use of the maximum power coefficient. Then it might be interesting to consider a combined

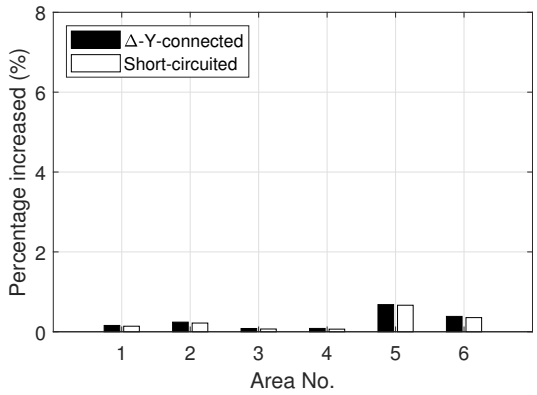

Fig. 21. AEP improvement only considering generator

mode in which the short-circuit mode for the low speed, the △-Y-connection mode for the medium speed, and the original DFIG operates at high speeds. This combination could be studied in future, but it might be too complicated for practical applications.

Secondly, Fig. 20 indicates that the areas with a low average wind speed benefit most from the presented methods. The AEP can increase by around 7% and 4% for Area 5 and Area 6, respectively, which are huge improvements. However, the AEP improvements in Area 3 and Area 4 are lower than 1%, which might not cover the cost for the additional equipment. With these quantified values, wind turbine manufacturers are at a better position to decide whether the presented improving methods can be adopted based on their wind farm locations.

The AEP evaluation is repeated. This time only considers the improvement of the generator efficiency. The other two advantages of extending the operating speed range and improving the aerodynamic efficiency are not considered. In other words, the shaft power keeps the same as the original DFIG based system. The results are summarized in Fig. 21. The increase is negligible. It means the increase of the generator efficiency at the low wind speed range plays a minor role in improving the AEP. The main advantage of applying the △-Y-connected and short-circuited DFIGs is to improve the aerodynamic conversion which finally increases the AEP.

V. Conclusions

The drivetrain improvement of the DFIG based wind turbines is barely investigated due to their maturity. The △-Y-connected and short-circuited DFIGs were previously proposed for higher generator efficiency at low loads. This paper applies the models of the aerodynamic, the gearbox, and the generator to elaborate these two methods from the perspective of the drivetrain energy conversion. The results indicate that only improving the generator efficiency makes little contribution to the AEP increase. More importantly, not only do these two methods decrease the cut-in speed, but also make the turbine rotor operate between an extended wind speed range with the optimal TSR. A higher power coefficient is then achieved at a low wind speed range.

The AEP evaluations are applied to six regions with different wind speed distributions. The results indicate that the

short-circuited DFIG performs better than the △-Y-connection mode for all regions. It increases the AEP much more in the areas with low average wind speed than that in the areas with high wind speed. In this case study, more specifically, the AEP is increased by about 7% in the low wind speed region (the average wind speed of about 3.2 m/s), while the increase is lower than 1% in the area with high wind speed (the average wind speed of 6∼7 m/s). Wind turbine manufacturers can apply the presented methods and evaluations to their wind farms. This study helps them decide whether the △-Y-connected or short-circuited DFIGs are worth for their particular applications. However, one interesting future work could be to investigate the transient process of the mode switching and the corresponding optimized control strategies in detail.

REFERENCES

[1] X. Song, C. Bührer, P. Brutsaert, and J. Krause *et al.*, "Designing and basic experimental validation of the world's first MW-class direct-drive superconducting wind turbine generator," *IEEE Transactions on Energy Conversion*, vol. 34, no. 4, pp. 2218–2225, Dec. 2019.

[2] X. Wang, T. D. Strous, D. Lahaye, H. Polinder, and J. A. Ferreira, "Modeling and optimization of brushless doubly-fed induction machines using computationally efficient finite-element analysis," *IEEE Transactions on Industry Applications*, vol. 52, no. 6, pp. 4525–4534, Nov./Dec. 2016.

[3] H. Polinder, "Overview of and trends in wind turbine generator systems," in *Power and Energy Society General Meeting, 2011 IEEE*, Jul. 2011, pp. 1–8.

[4] H. Polinder, J. A. Ferreira, B. B. Jensen, A. B. Abrahamsen, K. Atallah, and R. A. McMahon, "Trends in wind turbine generator systems," *Emerging and Selected Topics in Power Electronics, IEEE Journal of*, vol. 1, no. 3, pp. 174–185, Sept. 2013.

[5] Y. Chang, J. Hu, and X. Yuan, "Mechanism analysis of DFIG-based wind turbine's fault current during LVRT with equivalent inductances," *IEEE Journal of Emerging and Selected Topics in Power Electronics*, vol. 8, no. 2, pp. 1515–1527, Jun. 2020.

[6] N. Jabbour, E. Tsioumas, C. Mademlis, and E. Solomin, "A highly effective fault-ride-through strategy for a wind energy conversion system with a doubly fed induction generator," *IEEE Transactions on Power Electronics*, vol. 35, no. 8, pp. 8154–8164, Jun. 2020.

[7] A. Mishra, M. Singh, A. Srivastava, and K. Chatterjee, "Suppression of harmonics in DFIG based wece using passive LCL filter," in *2018 International Conference on Power Energy, Environment and Intelligen Control (PEEIC)*, Greater Noida, India, Apr. 2018.

[8] C. Wu and H. Nian, "Stator harmonic currents suppression for DFIG based on feed-forward regulator under distorted grid voltage," *IEEE Transactions on Power Electronics*, vol. 33, no. 2, pp. 1211–1224, Mar. 2017.

[9] B. Pang, H. Nian, C. Wu, and P. Cheng, "Stator harmonic current suppression for DFIG system considering integer harmonics and inter-harmonics," *IEEE Transactions on Industrial Electronics*, vol. 66, no. 9, pp. 7001–7011, Sept. 2019.

[10] N. V. Deshpande, K. Kalange, and S. Lokhande, "Output power maximization of wind energy conversion system using doubly fed induction generator," in *2018 8th IEEE India International Conference on Power Electronics (IICPE)*, Jaipur, India, Dec. 2018.

[11] M. N. Soares, J. Gyselinck, L. G. B. Rolim, J. Helsen, and Y. Mollet, "Loss minimisation strategy for DFIG in wind turbine considering iron losses," in *2018 IEEE International Conference on Industrial Technology (ICIT)*, Lyon, France, Feb. 2018.

[12] N. Karakasis, E. Tsioumas, N. Jabbour, A. M. Bazzi, and C. Mademlis, "Optimal efficiency control in a wind system with doubly fed induction generator," *IEEE Transactions on Power Electronics*, vol. 34, no. 1, pp. 356–368, Jan. 2019.

[13] E. Hau, *Wind Turbines, Fundamentals, Technologies, Application, Economics*. Springer-Verlag, 2013.

[14] A. Petersson, "Analysis, modeling and control of doubly-fed induction generators for wind turbines," Ph.D. dissertation, Chalmers University of Technology, 2005.

[15] A. C. Smith, R. Todd, M. Barnes, and P. J. Tavner, "Improved energy conversion for doubly fed wind generators," *IEEE Transactions on Industry Applications*, vol. 42, no. 6, pp. 1421–1428, Nov./Dec. 2006.

[16] A. Balogun, O. Ojo, and F. Okafor, "Shorted stator induction generator for low wind speed power application," in *IEEE PES General Meeting*, Providence, USA, Jul. 2010.

[17] F. Wei and D. M. Vilathgamuwa, "Mode switching DFIG for low voltage ride through," in *8th International Conference on Power Electronics - ECCE Asia*, Jeju, South Korea, Jun. 2011.

[18] A. Grauers, "Design of direct-driven permanent-magnet generators for wind turbines," Ph.D. dissertation, Chalmers University of Technology, 1996.

[19] J. Pyrhönen, T. Jokinen, and V. Hrabovcová, *Design of Rotating Electrical Machines*. John Wiley & Sons Ltd., 2007.

[20] G. Bertotti, "General properties of power losses in soft ferromagnetic materials," *IEEE Transactions on Magnetics*, vol. 24, no. 1, pp. 621–630, Jan. 1988.

[21] X. Lu and H. Wu, "Maximum efficiency control strategy for induction machine," in *ICEMS 2001 - 5th International Conference on Electrical Machines and Systems*, Aug. 2001.

[22] G. Abad, J. López, M. A. Rodríguez, L. Marroyo, and G. Iwanski, *Doubly Fed Induction Machine - Modeling and Control for Wind Energy Generation*. John Wiley & Sons Ltd., 2011.

[23] Y. Chang, J. Hu, W. Tang, and G. Song, "Fault current analysis of type-3 WTs considering sequential switching of internal control and protection circuits in multi time scales during LVRT," *IEEE Transactions on Power Systems*, vol. 33, no. 6, pp. 6894–6903, Nov. 2018.

[24] J. López, P. Sanchis, X. Roboam, and L. Marroyo, "Dynamic behavior of the doubly fed induction generator during three-phase voltage dips," *IEEE Transactions on Energy Conversion*, vol. 22, no. 3, pp. 709–717, Sept. 2007.

[25] A. Balogun, O. Ojo, and F. Okafor, "Efficiency optimization of doubly-fed induction generator transitioning into shorted-stator mode for extended low wind speed application," in *IECON 2013 - 39th Annual Conference of the IEEE Industrical Electronics Society*, Nov. 2013.

[26] Z. Yin, B. Bai, J. Liu, and S. Su, "Startup speed with dead band in wind farms with low-medium wind speed profile - case study of hong kong," *Energy and Pkwer Engineering*, vol. 9, no. 4B, pp. 562–572, Apr. 2017.

[27] J. Anthonis, A. Seuret, J. P. Richard, and H. Ramon, "Design of a pressure control system with dead band and time delay," *IEEE Trans. on Control Systems Technology*, vol. 15, no. 6, pp. 1103–1110, Nov. 2007.

[28] F. Liu, F. Sun, W. Liu, T. Wang, H. Wang, X. Wang, and W. H. Lim, "On wind speed pattern and energy potential in china," *Applied Energy*, vol. 236, pp. 867–876, Feb. 2019.

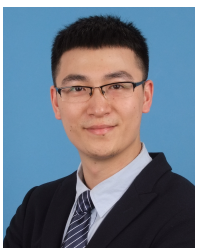

Xuezhou Wang (S'15-M'18) received the B.Sc. and M.Sc. degree in Electrical Engineering from Northwestern Polytechnical University, Xi'an, China, in 2010 and 2013, respectively, and the Ph.D. degree also in Electrical Engineering from Delft University of Technology, Delft, the Netherlands, in 2017. From 2017 to 2020, he worked as a senior electromagnetic design engineer at Envision Energy, Shanghai, China. Currently, he is working as a postdoc researcher in the field of hybrid/electric drivetrain systems for ship applications at Delft University of Technology. His current research interests include modeling and design of electrical machines, novel generators for wind turbines, and transportation electrification.

Dong Liu (S'13-M'18) received the bachelor's degree from Harbin Institute of Technology, Harbin, China, in 2007. He received the M.Sc. degree and Ph.D. degree from Delft University of Technology, Delft, the Netherlands, in 2012 and 2017, respectively. From 2017 to 2018, he was an electrical machine & power conversion engineer at XEMC Darwind BV, Hilversum, the Netherlands. Since 2018, he has been a research associate professor at Hohai University, Nanjing, China. His research interests are design of novel electrical machines for renewable energy conversion and applied superconductivity in electrical machines.

Henk Polinder (M'97-SM'13) received the Ph.D. degree in electrical engineering from Delft University of Technology, Delft, The Netherlands, in 1998. Since 1996, he has been an Assistant/ Associate Professor at Delft University of Technology, working in the field of electrical machines and drives. He worked part-time in industries, at wind turbine manufacturer Lagerwey from 1998 to 1999, at Philips CFT in 2001, and at ABB Corporate Research, Västerås, in 2008. He was a Visiting Scholar at Newcastle University, Newcastle upon Tyne, in 2002, at Laval University, Quebec, in 2004, at The University of Edinburgh in 2006, and the University of Itajubá in 2014. He has authored and co-authored of over 250 publications. His main research interests are electric drive and energy systems for maritime applications and offshore renewables.